MicroRNA Detection

DOI: 10.1002/ange.201108302

Target-Cell-Specific Delivery, Imaging, and Detection of Intracellular MicroRNA with a Multifunctional SnO_2 Nanoprobe**

Haifeng Dong, Jianping Lei, Huangxian Ju, Feng Zhi, Hua Wang, Wenjie Guo, Zhu Zhu, and Feng Yan**

MicroRNAs (miRNAs) are a class of short, endogenous, noncoding regulatory RNAs (approximately 18–25 nucleotides), encoded in the genomes of plants, animals, and viruses.[1–3] They partially complement the 3′ untranslated region of target mRNAs, causing mRNA cleavage or inhibiting protein synthesis within the Dicer/Argonaute complex.[4,5] MiRNAs play key regulatory roles in a diverse range of biological processes, including cell development,[6] differentiation,[7] metabolism,[8] and apoptosis.[9] In particular, distinct miRNA expression patterns are associated with various cancer phenotypes.[10–12] Therefore, miRNAs are also an emerging class of useful diagnostic and prognostic markers.[13–15] However, miRNA analysis is challenging owing to the unique characteristics of miRNAs, such as their small size, sequence similarity among family members, low abundance, susceptibility to degradation, and the technical impediments in delivering miRNAs across the plasma membrane of cells. An improved delivery strategy is thus needed to successfully monitor intracellular miRNA levels in situ.[16,17]

Generally, transmission of oligonucleotides for gene therapy falls into two broad categories, viral vectors[18,19] or nonviral carriers.[20–24] Viral vectors exhibit high transfection efficiency but also some fundamental problems, such as immunogenicity and toxicity. These problems limit their broad application.[18,19] Currently, the nonviral vectors, such as liposomes,[20] cationic polymers,[21] dendrimers,[22] polypeptides,[23] and nanomaterials[24] have attracted significant interest, owing to their good biocompatibility and potential for large-scale production, in contrast to viral vectors.[25] However, many of these carrier systems do not inhibit genes in a cell-specific manner and cannot be used to monitor their intracellular delivery or therapeutic response.[26,27] An excellent nonviral vector should efficiently facilitate cell-specific gene-probe (a single-stranded oligonucleotide designed to recognize a single target-nucleotide sequence) uptake and gene-probe endosomal escape for intracellular delivery.[28] Fluorescent nanoparticles are highly attractive materials for gene-probe delivery because of their unique properties, including uniform size, superior imaging characteristics, and facile surface modification.[29,30] The rational functionalization of these nanomaterials with target-specific moieties, such as antibodies,[31] aptamers,[32] and other molecules,[33] to recognize receptors on the cell surface has led to versatile theragnostic nanosystems. These multifunctional nanosystems not only allow efficient delivery of gene probes to target cells with fewer side effects, but also allow the simultaneous monitoring of delivery and the therapeutic response of the targeted genes, using the advanced optical properties of the nanosystem. However, these nanosystems have not been used for in situ detection of intracellular miRNAs yet, because the detection strategy has not been optimized.

In this study we design a novel multifunctional SnO_2 nanoprobe (mf-SnO_2), which contains a cell-targeting moity, as well as a conjugated gene probe to specifically recognize the target sequence, thus providing a detection strategy or inhibitor. Also, visualization of the delivery and intracellular response is possible through fluorescence of the SnO_2. As shown in Scheme 1, cell-specific delivery is achieved by functionalizing SnO_2 nanoparticles (SnO_2NPs) with folic acid (FA), which targets cancer cells; a gene probe, in this case a molecular beacon (MB) to detect target miRNAs, is conjugated by a disulfide linkage, which is sensitive to pH values. Cleavage of the disulfide linkage between the gene probe and the nanoparticle enhances the efficiency of intracellular delivery.[26,34] Using miRNA-21 in HeLa cells as a model, a method for in situ detection of intracellular miRNA by the multifunctional nanoprobe is reported.

To verify the practicality of this approach, another nanoprobe was also designed, by substituting the MB with an anti-miR of miRNA-21, to down-regulate the expression of a target miRNA. The proposed method, with a MB as the recognition probe, can be used subsequently to monitor the change in miRNA levels from negligible cytotoxicity, and to monitor the ability of the multifunctional nanoprobe to

[*] Dr. H. Dong, Prof. J. Lei, Prof. H. Ju, Z. Zhu
State Key Laboratory of Analytical Chemistry for Life Science, School of Chemistry and Chemical Engineering, Nanjing University
Nanjing 210093 (P.R. China)
E-mail: hxju@nju.edu.cn
Dr. F. Zhi, Dr. W. Guo
State Key Laboratory of Pharmaceutical Biotechnology
School of Life Science, Nanjing University
Nanjing 210093 (P.R. China)
Dr. H. Wang
School of Chemistry and Environment
Beijing University of Aeronautics & Astronautics
Beijing 100191 (P.R. China)
Prof. F. Yan
Jiangsu Institute of Cancer Prevention and Cure
Nanjing 210009 (P. R. China)
E-mail: yanfeng2007@sohu.com

[**] We gratefully acknowledge National Basic Research Program (2010CB732400), National Natural Science Foundation of China (21075055, 21135002, 21121091), and Leading Medical Talents Program from Department of Health of Jiangsu Province.

Supporting information for this article is available on the WWW under http://dx.doi.org/10.1002/anie.201108302.

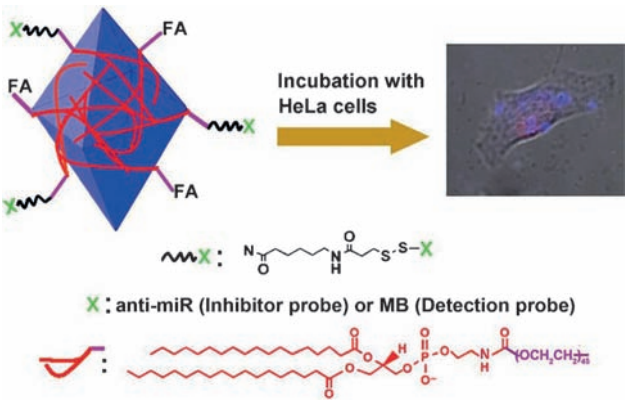

Scheme 1. Schematic representation of mf-SnO_2 nanoprobe for target-specific-cell imaging and intracellular detection of miRNA. FA = folic acid, MB = molecular beacon.

protect gene probes from nuclease digestion or interaction with single-stranded DNA binding protein (SSB).

The structure of SnO_2NPs was confirmed by X-ray diffraction (XRD; Figure S1, Supporting Information). All of the peaks in the XRD pattern could be indexed to the rutile phase of SnO_2 (JCPDS No. 41-1445). The scanning electron microscope (SEM) image of the SnO_2NPs showed a well-proportioned octahedral structure with surface roughness. The size of the NPs was estimated to be approximately 60 nm in width and 80 nm in length (Figure 1a). The transmission electron microscope (TEM) image taken from the apex of the nanoparticle along the [110] direction further demonstrated an octahedral structure and confirmed the estimated size (Figure 1b), which was in agreement with reported values.[35] Dynamic light scattering (DLS) measurements showed the hydrodynamic diameter of the SnO_2NPs to be about 80 nm with a narrow size distribution (Figure 1c). Also, Brunauer–Emmett–Teller adsorption–desorption isotherm curves showed that the SnO_2NPs were porous, with an average pore diameter of 10.4 nm (Figure S2, Supporting Information). The SnO_2NPs emitted strong photoluminescence, with a band at 467 nm and a full-width at half maximum (FWHM) of 40 nm (Figure S3, Supporting Information).

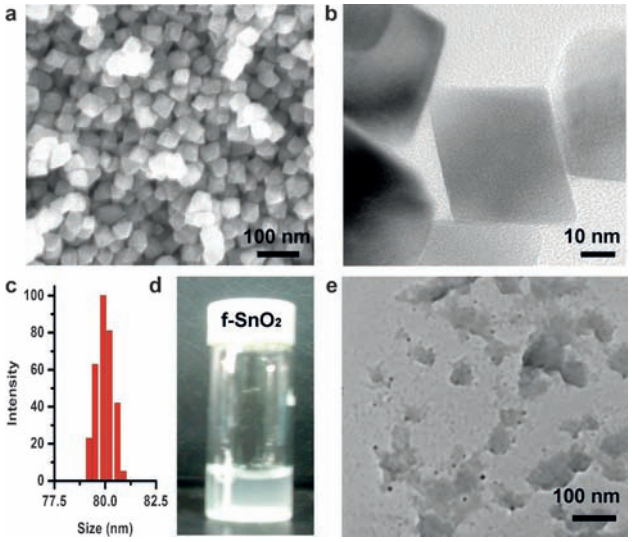

Figure 1. a) SEM, b) TEM, and c) DLS characterization of SnO_2NPs. d) f-SnO_2, functionalized with DL-PEG_{2000}-FA and DL-PEG_{2000}-SPDP, in PBS (pH 7.2, 0.1 M) containing serum proteins (10%). e) TEM image of f-SnO_2.

A stable aqueous suspension of SnO_2NPs could be obtained by noncovalently functionalizing the SnO_2NPs with 1,2-distearoyl-*sn*-glycero-3-phosphoethanolamine-*N*-[amino (polyethylene glycol)$_{2000}$] (DL-PEG_{2000}) conjugated to FA (DL-PEG_{2000}-FA) or sulfosuccinimidyl-6-(3′(2-pyridyldithio)propionamido)hexanoate (DL-PEG_{2000}-SPDP; Figure 1d). These moieties were adsorbed on the nanoparticles through van der Waals and hydrophobic interactions.[36] The hydrophilic PEG chain extended into the aqueous phase to solubilize the DL-PEG_{2000}-FA- and DL-PEG_{2000}-SPDP-functionalized SnO_2NPs (f-SnO_2) in phosphate buffered saline (PBS) containing serum proteins (Figure 1e), which approximates physiological conditions. Compared to the SnO_2NPs, the TEM image of f-SnO_2 showed a smooth surface and increased size (Figure 1e). The appropriate size and good fluorescent properties combined with the stable solubility under physiological conditions, make the SnO_2NP a promising carrier for oligonucleotides. The zeta-potential analysis and electrochemical impedance spectrum analysis confirmed that SnO_2NPs were successfully functionalized with both DL-PEG_{2000}-FA and DL-PEG_{2000}-SPDP-MB (gene probe, Figure S4, Supporting Information).

Oligonucletides, such as anti-miR, are susceptible to degradation by cellular nucleases during delivery into the cells.[37–39] Therefore, an efficient delivery vector should protect the cargo against nuclease digestion and SSB interaction during prolonged transport. Herein, the ability of multifunctionalized SnO_2NPs (mf-SnO_2) to resist nuclease cleavage and SSB interaction during the recognition of the target sequence by the MB was examined. After incubating the mixture of mf-SnO_2 and miRNA-21, a sharp increase of fluorescence from the carboxyfluorescein (FAM) labeled MB was observed (Figure S5, Supporting Information), indicating specific recognition of miRNA-21 and successful conjugation of f-SnO_2 with the MB. DNase I nuclease digestion and SSB interaction experiments demonstrated that the mf-SnO_2 nanoprobe could protect the MB from nucleases (Figure S6A, Supporting Information) and interfering proteins (Figure S6B, Supporting Information). The protective effect could be from shielding by the f-SnO_2 and/or the conformational change of nucleic acid strands in the presence of f-SnO_2, both of which have been seen with carbon nanotubes.[40,41]

The cytotoxicity of f-SnO_2 was studied using 3-(4,5-dimethylthiazol-2-yl)-2,5-diphenyltetrazolium bromide (MTT) assay and an apoptosis assay. As a control, the cytotoxicity of commercial transfection agents, Lipofectamine 2000 (Lp2000) and polyethyleneimine (PEI), was also evaluated. The f-SnO_2 displayed low cytotoxicity with HeLa cells in the range from 20 mg L^{-1} to 320 mg L^{-1} (Figure 2a). The f-SnO_2-transfected cells showed 94.9% viability at the concentration of 100 mg L^{-1}, while the cells treated with PEI and Lp2000 exhibited 88.7% and 84.8% viability, respectively (Figure 2b), indicating lower cytotoxicity of the NPs, although the error in these measurements is not sufficient to

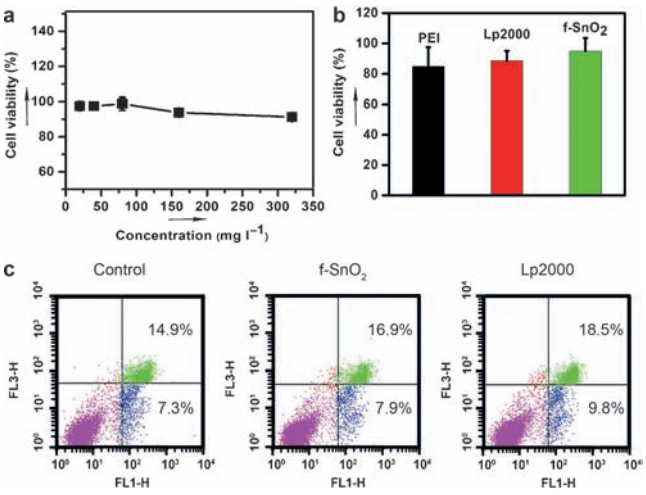

Figure 2. a) Cytotoxicity induced by f-SnO_2 at different concentrations (20, 40, 80, 160, 320 mg L^{-1}) in HeLa cells. b) Cytotoxicity induced by PEI (0.05 mM), Lp2000 (0.2 μL per 100 μL medium) and f-SnO_2 (100 mg L^{-1}). c) Flow-cytometric analysis of apoptosis in HeLa cells and HeLa cells transfected by f-SnO_2 (100 mg L^{-1}) or Lp2000 (0.2 μL per 100 μL medium). Normal cells (purple), apoptotic cells in late phase (green) and in early phase (blue); FL1-H = Annexin V positive cells, FL3-H = PI positive cells.

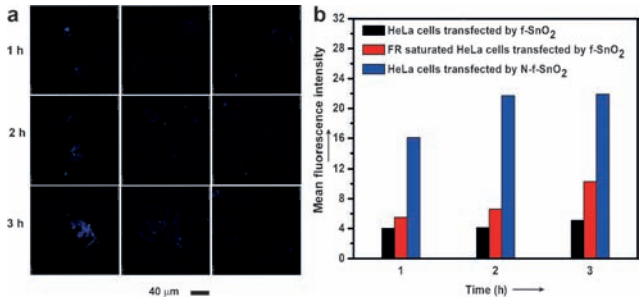

Figure 3. a) Confocal images of HeLa cells transfected with f-SnO_2 (left, 100 mg L^{-1}), FR-saturated HeLa cells transfected with f-SnO_2 (middle, 100 mg L^{-1}), and HeLa cells transfected with N-f-SnO_2 (right, 100 mg L^{-1}) at 37 °C at marked times. b) Corresponding fluorescence intensities of (a). Blue field = SnO_2NP fluorescence.

establish statistical significance. The lower cytotoxicity of f-SnO_2 than both PEI and Lp2000 could result from the negative surface charge, which will lower NP adhesion to the cell surface, decreasing the necrosis that is seen with positively charged PEI.[42] The difference in cytotoxicity could also be attributed to the nontoxic composition of f-SnO_2, unlike some quantum dots containing toxic elements, such as cadmium.[43,44] In comparison to the control group with 7.3% of cells being apoptotic, 7.9% of f-SnO_2-transfected cells were apoptotic, according to Annexin V-FITC and propidium iodide(PI)-labeling flow-cytometry analysis (Figure 2c). The f-SnO_2 displayed 20% lower apoptosis than the commercial transfection agent Lp2000. These results suggest that f-SnO_2 is a relatively safe transfection agent.

In principle, it is possible to employ the fluorescent f-SnO_2 for live-cell imaging and monitoring of the intracellular transfection efficiency (Figure S7, Supporting Information). Target-cell-specific delivery has been regarded as important for the development of therapeutics, because it can limit side effects from nonspecific delivery and reduce the quantity of gene probe needed for treatment.[45] Herein FA, a ligand with high affinity to the folate receptor (FR), which is overexpressed on many human cancer cells causing rapid proliferation,[46] was conjugated to the SnO_2NPs as a target-specific moiety. To confirm the specific FR-mediated transfection of the f-SnO_2, competitive binding tests with free FA and the transfection of f-SnO_2 without the presence of FA (N-f-SnO_2) were carried out. As expected, a gradual increase of fluorescence intensity, which came from the emission of the SnO_2NPs, was observed in the f-SnO_2 transfected cells, indicating the gradual uptake of the f-SnO_2 (Figure 3a, left column). In contrast, fluorescence was almost undetectable after the cells were treated with free FA for 1 hour and then transfected with the f-SnO_2 (Figure 3a, middle column). The lack of f-SnO_2 uptake was due to the occupancy of FRs on the cell surface by free FA molecules, which reduced the receptor-mediated endocytosis.[47] In absence of FA, the transfection of N-f-SnO_2 also showed little uptake (Figure 3a, right column), indicating the nonspecific uptake of nanoparticles was negligible. The mean fluorescence intensities per cell are shown in Figure 3b, which highlights the differences in the uptake of f-SnO_2. FA receptor-negative A549 cells and FA receptor-positive MCF-7 cells also were treated with f-SnO_2 under similar conditions to the HeLa cells; higher fluorescence was detected in MCF-7 cells, further verifying the FR-mediated endocytosis of f-SnO_2 (Figure S8, Supporting Information). The FA-conjugated SnO_2NPs could be used as a target-cell-specific transfection reagent.

To evaluate the transfection capability of f-SnO_2 into HeLa cells, a transfection probe (TP: a FAM-labeled, single-stranded DNA of random sequence, see Supporting information) was conjugated to f-SnO_2 using a disulfide linkage. After the resulting mf-SnO_2-TP (also conjugated with FA) was internalized into cells by FR-mediated endocytosis, the disulfide linkage between TP and f-SnO_2 can be cleaved in the reductive and acidic intracellular environment[47–49] to release the TP (Figure S9, Supporting Information), which enhanced the efficiency of intracellular delivery.[50] The internalization could be confirmed by the TEM images, while the confocal microscopic images indicated some cleavage of the mf-SnO_2-TP (Figure S10, Supporting Information). The transfection efficiency of mf-SnO_2-TP (100 mg L^{-1}, 50 nM linked TP) was assessed in comparison to a commercial transfection agent Lp2000-TP (0.2 μL per 100 μL medium, 50 nM TP) and a typical polymeric vector[21] PEI-TP (0.05 mM, 50 nM TP). The results indicated the promising transfection efficiency of the mf-SnO_2-TP (Figure S11, Supporting Information).

MiRNA mutation or disregulation is associated with various human cancers.[51,52] Thus, methods to detect or inhibit intracellular miRNAs are useful in finding new biomarkers for clinical diagnosis and new targets for gene therapy. Using miRNA-21, linked to several cancers,[53,54] as a model, the inhibitor probe anti-miR of miRNA-21 was conjugated to f-SnO_2 by disulfide bond, to down-regulate the level of the miRNA-21. The intracellular miRNA-21 level was monitored

by confocal microscopy after target-cell-specific delivery of mf-SnO_2-MB into the cells. After the cells were incubated with the FA-conjugated mf-SnO_2-anti-miR for 48 h to inhibit the miRNA expression, the fluorescence intensity of FAM-labeled MB was 40.9% of that without miRNA-21 down-regulation (Figure 4, red field). This result was verified by reverse-transcriptase quantitative PCR (RT-PCR) analysis, which showed 49.4% down-regulation (Figure S12, Supporting Information). Thus, the designed multifunctional SnO_2 nanoparticle could be used for both regulation and in situ monitoring of intracellular miRNA levels.

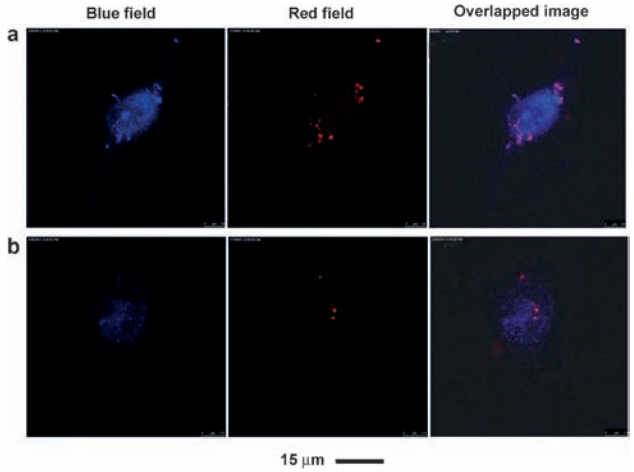

Figure 4. a) Confocal images of HeLa cells transfected with mf-SnO_2-MB (100 mg L^{-1}, 50 nM linked MB) at 37°C for 3 h. b) HeLa cells first transfected by mf-SnO_2-anti-miR (100 mg L^{-1}, 50 nM linked anti-miR) at 37°C for 3 h and detected with mf-SnO_2-MB (100 mg L^{-1}, 50 nM linked MB) 48 h later. Red field = FAM-labeled MB, blue field = SnO_2NP fluorescence.

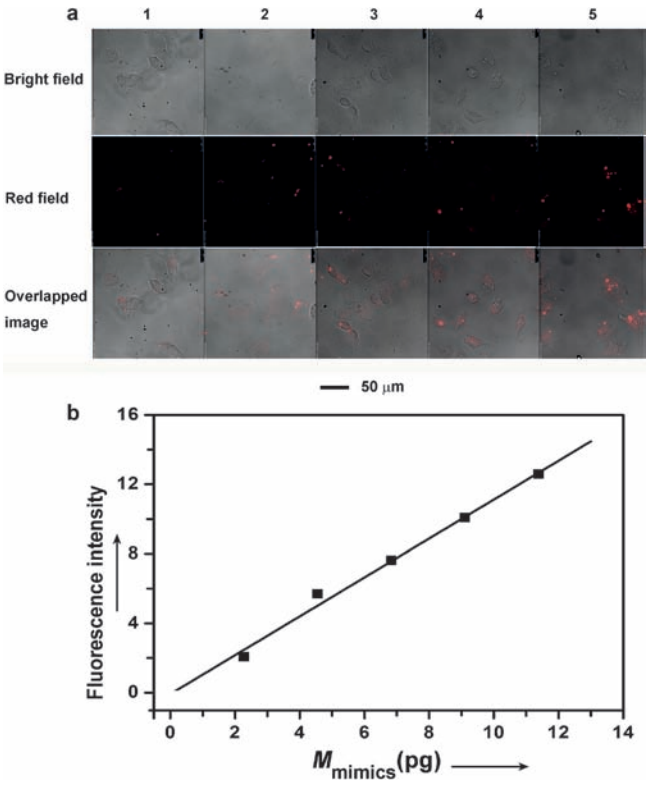

Figure 5. a) Confocal images of HeLa cells transfected with Lp2000-miRNA-21-mimics (0.2 μL per 100 μL medium) mixed with different amounts of miRNA-21 mimics (the quantity internalized by a single HeLa cell was 2.27, 4.55, 6.83, 9.11 and 11.38 pg from 1 to 5, respectively) at 37°C for 3 h, then detected with mf-SnO_2-MB (100 mg L^{-1}, 50 nM linked MB). b) Plot of fluorescence intensity versus quantity of intracellular miRNA-21 mimics.

To assess detection of intracellular miRNA, different amounts of miRNA-21 mimics (Sequences found in the Supporting information; http://microrna.sanger.ac.uk/sequences) were transfected into the cells, which were then transfected with mf-SnO_2-MB to obtain a calibration curve. The red fluorescence intensity, measured by confocal microscopy, increased with increasing amount of miRNA-21 mimics in the cells, (Figure 5a). The plot of fluorescence intensity versus the amount of miRNA-21 mimics transfected into a single cell, up to 11.3 pg, showed a linear relationship, with a related coefficient of 0.995 (Figure 5b). From the linear regression equation and the fluorescence intensity of FAM from the HeLa cells, the average quantity of miRNA-21 in a single HeLa cell can be calculated as 1.63 pg. All of these experiments describe an effective imaging method for in situ detection of intracellular miRNA.

In summary, this work develops a multifunctional SnO_2 nanoprobe for simultaneous specific delivery, cell imaging and intracellular miRNA detection. The mf-SnO_2 nanoparticle can protect conjugated oligonucleotides from nuclease digestion and SSB interaction during in vitro cellular delivery. MTT and apoptosis assays indicate the low cytotoxicity of the f-SnO_2. The FR-mediated endocytosis and cell-specific targeting of f-SnO_2 by FA conjugation has been verified. An appropriate size, good fluorescent properties, solubility under physiological conditions, and high transfection efficiency make f-SnO_2 a promising target-cell-specific transfection agent. The f-SnO_2 has been further functionalized with different oligonucleotides, including a transfection probe, an inhibition probe, and a detection probe, which suggests future applications in regulating the expression of intracellular miRNA levels and in situ monitoring of the change in miRNA levels. A novel method for in situ detection of miRNAs in a single cell has also been proposed. Both the multifunctional SnO_2 nanoprobe and the methods used in this report can be applied in biomedical and clinical research.

Experimental Section

The HeLa cell line was obtained from the Jiangsu Institute of Cancer Prevention and Cure, Nanjing, China. A549 and MCF-7 cell lines were kindly provided by School of Life Science, Nanjing University. All the three cell lines were cultured in Dulbecco's modified Eagle's medium (DMEM, GIBCO) supplemented with 10% fetal calf serum, penicillin (100 mg mL^{-1}), and streptomycin (100 mg mL^{-1}) at 37°C in a humidified atmosphere containing 5% CO_2. Cell numbers were obtained using a Petroff–Hausser cell counter (USA). Serum-free medium (Opti-MEM) was used during the transfection process.

The HeLa cells (1.0×10^4) were cultured for 12 h in a 96-well plate containing DMEM (100 μL) in each well, the medium was replaced with fresh Opti-MEM alone or medium containing f-SnO_2 (100 mg L^{-1}), Lp2000 (0.2 μL per 100 μL medium), or PEI (0.05 mM) to incubate for another 3 h. MTT (100 μL, 1 mg mL^{-1}) was then added to each well. The media were removed 4 h later, and sodium dodecylsulfate (150 μL, 0.52 M) was added to solubilize the formazan dye. After 15 min, the absorbance of each well was measured using Hitachi/Roche System Cobas 6000 (Tokyo, Japan) at 490 nm. The relative cell viability (%) was calculated by (A_{test}/$A_{control}$) × 100.

The apoptosis experiments were carried out with Annexin V-FITC/PI double staining. The cells (1.6×10^5) were seeded for 12 h in a 6-well plate containing DMEM (2 mL) in each well. The culture medium was then replaced with Opti-MEM (2 mL) containing f-SnO_2 (100 mg L^{-1}), Lp2000 (0.2 μL per 100 μL medium), or PEI (0.05 mM) and cultured for another 3 h. After discarding the medium, fresh DMEM was added, and cells incubated for another 24 h. The resulting cells were harvested, and stained with Annexin V-FITC/PI for 10 min, according to manufacturer's instruction. The HeLa cells were then collected and analyzed by flow cytometry on FACS Calibur flow cytometer (Becton Dickinson, USA).

The target-cell-specific transfection was performed as follows: after HeLa cells were cultivated for 12 h in 24-well culture plates containing DMEM (500 μL), with an initial 4×10^4 cells/well, the medium was replaced with fresh Opti-MEM (500 μL) containing f-SnO_2 (100 mg L^{-1}) or N-f-SnO_2 (100 mg L^{-1}) at room temperature for 3 h. For the competitive test, prior to transfection with f-SnO_2 (100 mg L^{-1}), the cells were first incubated with Opti-MEM (500 μL) containing FA (1 mM) for 1 h, to saturate the FR sites on the cell surface. The transfection of MCF-7 and A549 cells with f-SnO_2 was carried out using the same procedure.

For analysis of intracellular miRNAs with mf-SnO_2-MB, HeLa cells were cultivated on glass cover slides for 12 h, at an initial density of 4×10^4 cells/slide, which were transferred into 24-well culture plates containing DMEM (500 μL) in each well. The medium was then replaced with fresh Opti-MEM (500 μL) containing mf-SnO_2 (100 mg L^{-1}, 50 nM linked MB) and cultivated for 3 h. Prior to performing the confocal imaging, the cover slides were washed thoroughly and fixed on glass slides. In the inhibitor experiment, HeLa cells were first transfected with mf-SnO_2-anti-miR (100 mg L^{-1}, 50 nM linked inhibitor probe anti-miR) at 37 °C for 3 h and then 48 h later transfected with mf-SnO_2-MB (100 mg L^{-1}, 50 nM linked MB), for detection. To detect the amount of intracellular miRNA in situ, the cells were first incubated with Opti-MEM (500 μL) containing Lp2000-miRNA-21-mimics (0.2 μL per 100 μL medium) and different amounts of miRNA-21 mimics and 48 h later detected with mf-SnO_2-MB (100 mg L^{-1}, 50 nM linked MB). The quantity of miRNA mimics internalized by a single HeLa cell was calculated by ($M_{before} - M_{after}$)/A_{cell} number, where M_{before} and M_{after} was the mass of mimics in the media before and after transfection calculated by the absorbance at 260 nm, respectively, and A_{cell} number was the number of transfected cells.

The details about preparation, functionalization, and characterization of SnO_2NPs, assembly and characterization of mf-SnO_2, response of mf-SnO_2-MB to target in vitro, protection properties of f-SnO_2, in vivo transfection by f-SnO_2, FA-mediated endocytosis of f-SnO_2, gel electrophoresis experiments, in vivo transfection by mf-SnO_2-TP, transfection efficiency, and reverse-transcriptase quantitative PCR (RT-qPCR) experiments are described in the Supporting Information.

Received: November 24, 2011
Revised: February 28, 2012
Published online: March 30, 2012

Keywords: gene vector · imaging · microRNA detection · multifunctional nanoprobe · SnO_2 nanoparticles

[1] P. Landgraf, M. Rusu, R. Sheridan, A. Sewer, N. Iovino, A. Aravin, *Cell* **2007**, *129*, 1401.
[2] A. C. Mallory, H. Vaucheret, *Nat. Genet.* **2006**, *38*, S31.
[3] B. R. Cullen, *Nat. Genet.* **2006**, *38*, S25.
[4] V. Ambros, *Nature* **2004**, *431*, 350.
[5] D. P. Bartel, *Cell* **2004**, *116*, 281.
[6] R. H. Plasterk, *Cell* **2006**, *124*, 877.
[7] M. V. Joglekar, V. M. Joglekar, A. A. Hardikar, *Gene Expression Patterns* **2009**, *9*, 109.
[8] P. Xu, S. Y. Vernooy, M. Guo, B. A. Hay, *Curr. Biol.* **2003**, *13*, 790.
[9] J. Brennecke, D. R. Hipfner, A. Stark, R. B. Russell, S. M. Cohen, *Cell* **2003**, *113*, 25.
[10] H. Grosshans, W. Filipowicz, *Nature* **2008**, *451*, 414.
[11] E. Stahlhut, E. Carlos, F. J. Slack, *Yale J. Biol. Med.* **2006**, *79*, 131.
[12] G. A. Calin, C. M. Croce, *Nat. Rev. Cancer* **2006**, *6*, 857.
[13] M. S. Kumar, J. Lu, K. L. Mercer, T. R. Golub, T. Jacks, *Nat. Genet.* **2007**, *39*, 673.
[14] S. Volinia, G. A. Calin, C. G. Liu, S. Ambs, A. Cimmino, F. Petrocca, R. Visone, M. Iorio, C. Roldo, M. Ferracin, R. L. Prueitt, N. Yanaihara, G. Lanza, A. Scarpa, A. Vecchione, M. Negrini, C. C. Harris, M. C. Croce, S. Volinia, *Proc. Natl. Acad. Sci. USA* **2006**, *103*, 2257.
[15] A. Gupta, J. J. Gartner, P. Sethupathy, A. G. Hatzigeorgiou, N. W. Fraser, *Nature* **2006**, *442*, 82.
[16] Y. Q. Cheng, X. Zhang, Z. P. Li, X. X. Jiao, Y. C. Wang, Y. L. Zhang, *Angew. Chem.* **2009**, *121*, 3318; *Angew. Chem. Int. Ed.* **2009**, *48*, 3268.
[17] W. P. Kloosterman, E. Wienholds, E. D. Bruijn, S. Kauppinen, R. H. A. Plasterk, *Nat. Methods* **2006**, *3*, 27.
[18] D. H. Palmer, L. S. Young, V. Mautner, *Trends Biotechnol.* **2006**, *24*, 76.
[19] N. V. Somia, T. Kafri, I. M. Verma, *Nat. Biotechnol.* **1999**, *17*, 224.
[20] O. Zelphati, F. C. Szoka, *Proc. Natl. Acad. Sci. USA* **1996**, *93*, 11493.
[21] O. Boussif, F. Lezoualc'h, M. A. Zanta, M. D. Mergny, D. Scherman, B. Demeneix, J. P. Behr, *Proc. Natl. Acad. Sci. USA* **1995**, *92*, 7297.
[22] A. Harada, M. Kawamura, T. Matsuo, T. Takahashi, K. Kono, *Bioconjugate Chem.* **2006**, *17*, 3.
[23] S. L. Lo, S. Wang, *Biomaterials* **2008**, *29*, 2408.
[24] R. Singh, D. Pantarotto, D. McCarthy, O. Chaloin, J. Hoebeke, C. D. Partidos, J. P. Briand, M. Prato, A. Bianco, K. Kostarelos, *J. Am. Chem. Soc.* **2005**, *127*, 4388.
[25] H. F. Dong, L. Ding, F. Yan, H. X. Ji, H. X. Ju, *Biomaterials* **2011**, *32*, 3875.
[26] A. M. Derfus, A. A. Chen, D. H. Min, E. Ruoslahti, S. N. Bhatia, *Bioconjugate Chem.* **2007**, *18*, 1391.
[27] S. H. Lee, S. H. Choi, S. H. Kim, T. G. Park, *J. Controlled Release* **2008**, *125*, 25.
[28] H. Hatakeyama, H. Akita, H. Harashima, *Adv. Drug Delivery Rev.* **2011**, *63*, 152.
[29] Y. S. Choi, H. P. Kim, S. M. Hong, J. Y. Ryu, S. J. Han, R. Song, Y. S. Choi, *Small* **2009**, *5*, 2085.
[30] C. C. Chen, Y. C. Liu, C. H. Wu, C. C. Yeh, M. T. Su, Y. C. Wu, *Adv. Mater.* **2005**, *17*, 404.
[31] E. Song, P. C. Zhu, S. K. Lee, D. P. J. Chowdhhury, S. Kussman, D. M. Dykxhoorn, Y. Feng, D. Palliser, D. B. Weiner, P. Shankar, W. A. Marasco, J. Lieberman, *Nat. Biotechnol.* **2005**, *23*, 709.
[32] O. J. McNamara II, E. R. Andrechek, Y. Wang, K. D. Viles, E. R. Rachel, E. Gilboa, B. A. Sullenger, P. H. Giangrande, *Nat. Biotechnol.* **2006**, *24*, 1005.
[33] M. Ogris, G. Walker, T. Blessing, R. Kircheis, M. Wolschek, E. Wagner, *J. Controlled Release* **2003**, *91*, 173.

[34] S. Nayak, H. M. Lee, J. Chmielewski, L. Lyon, *J. Am. Chem. Soc.* **2004**, *126*, 10258.
[35] H. Wang, Y. M. Wu, Y. S. Bai, W. Zhou, Y. R. An, J. H. Li, L. Guo, *J. Mater. Chem.* **2011**, *21*, 10189.
[36] W. S. Seo, J. H. Lee, X. M. Sun, Y. Suzuki, D. Mann, Z. Liu, M. Terashima, P. C. Yang, M. V. McConnell, D. G. Nishimura, H. J. Dai, *Nat. Mater.* **2006**, *5*, 971.
[37] D. Cai, J. M. Mataraza, Z. H. Qin, Z. P. Huang, J. Y. Huang, T. C. Chiles, D. Carnahan, K. Kempa, Z. F. Ren, *Nat. Methods* **2005**, *2*, 449.
[38] V. Sokolova, M. Epple, *Angew. Chem.* **2008**, *120*, 1402; *Angew. Chem. Int. Ed.* **2008**, *47*, 1382.
[39] X. X. He, K. M. Wang, W. H. Tan, B. Liu, X. Lin, C. M. He, D. Li, S. S. Huang, J. Li, *J. Am. Chem. Soc.* **2003**, *125*, 7168.
[40] Y. R. Wu, J. A. Phillips, H. P. Liu, R. H. Yang, W. H. Tan, *ACS Nano* **2008**, *2*, 2023.
[41] M. Zheng, A. Jagota, E. D. Semke, B. A. Diner, R. S. Mclean, S. R. Lustig, R. E. Richardson, N. G. Tassi, *Nat. Mater.* **2003**, *2*, 338.
[42] D. Fischer, T. Bieber, Y. Li, H. P. Elsasser, T. Kissel, *Pharm. Res.* **1999**, *16*, 1273.
[43] S. Prakash, S. Rao, C. Dameron, *Biochem. Biophys. Res. Commun.* **1998**, *244*, 198.
[44] Z. Hossain, F. Huq, *J. Inorg. Biochem.* **2002**, *90*, 85.
[45] K. Kogure, R. Moriguchi, K. Sasaki, M. Ueno, S. Futaki, H. Harashima, *J. Controlled Release* **2004**, *98*, 317.
[46] Y. J. Lu, P. S. Low, *Adv. Drug Del. Rev.* **2002**, *90*, 85.
[47] D. J. Bharali, D. W. Lucey, H. Jayakumar, H. E. Pudavar, P. N. Prasad, *J. Am. Chem. Soc.* **2005**, *127*, 11364.
[48] G. Saito, J. A. Swanson, K. D. Lee, *Adv. Drug Delivery Rev.* **2003**, *55*, 199.
[49] X. Chen, A. Kis, A. Zett, C. R. Bertozzi, *Proc. Natl. Acad. Sci. USA* **2007**, *104*, 8218.
[50] Y. Bae, S. Fukushima, A. Harada, K. Kataoka, *Angew. Chem.* **2003**, *115*, 4788; *Angew. Chem. Int. Ed.* **2003**, *42*, 4640.
[51] S. M. Johnson, H. Grosshans, J. Shingara, M. Byrom, R. Jarvis, A. Cheng, E. Labourier, K. L. Reinert, D. Brown, F. J. Slack, *Cell* **2005**, *120*, 635.
[52] K. A. O'Donnell, E. A. Wentzel, K. I. Zeller, C. V. Dang, J. T. Mendell, *Nature* **2005**, *435*, 839.
[53] L. F. Sempere, M. Christensen, A. Silahtaroglu, M. Bak, C. V. Heath, G. Schwartz, W. Wells, S. Kauppinen, C. N. Cole, *Cancer Res.* **2007**, *67*, 11612.
[54] J. A. Chan, A. M. Krichevsky, K. S. Kosik, *Cancer Res.* **2005**, *65*, 6029.

